

1

Supplementary Information

2 **Atomically Dispersed Iron-Zinc Dual-Metal Sites to Boost Catalytic**

3 **Oxygen Reduction Activities for Efficient Zinc-Air Batteries**

4 Zi-Han Zhao^{a,b}, Dakai Ma^{a,b}, Zhuang Zewen^{a,b}, Kaili Wang^{a,b}, Xu Chenhui^{a,b}, Sun kaian^{a,b}, Deng Shu-Qi^{a,b*}, Wei
5 Yan^{a,b*}, and JiuJun Zhang^{a,b*}

6

7 *a School of Materials Science and Engineering, Fuzhou University, Fuzhou City, Fujian Province, 350108, P.R China*

8 *b Fujian Engineering Research Center of High Energy Batteries and New Energy Equipment & Systems, Fuzhou University, Fuzhou City, Fujian Province,*
9 *350108, P.R China*

10

11

* Corresponding authors.

E-mail: deng_shuqi@126.com (Shu-Qi Deng); weiyang@fzu.edu.cn (Wei Yan); jiuJun.zhang@fzu.edu.cn (JiuJun Zhang).

1 Table of Contents

2	Supplementary Notes	3
3	Chemicals and Materials	3
4	Characterizations	3
5	Electrochemical Measurements.....	4
6	Fabrication and Measurements of Zn-air Battery.....	6
7	Supplementary Figures.....	7
8	Supplementary Tables	22
9		

1 Supplementary Notes

2 Chemicals and Materials

3 All chemicals were used as received without any purification. Zinc acetate dihydrate
4 ($\text{Zn}(\text{OAc})_2 \cdot 2\text{H}_2\text{O}$, AR, 99%), terephthalic acid (H^2BDC , 99%), N, N-dimethylformamide (DMF,
5 AR, 99.5%), triethylamine (Et^3N , AR, 99.0%), Iron(II) acetate ($\text{Fe}(\text{OAc})_2$, 90.0%(T)), Potassium
6 hydroxide (KOH, Electronic grade, 99.9%), propane-2-ol (99.9%), Polyvinylpyrrolidone (PVP,
7 M.W.~40,000, high grade pure, K30) and 1,10-phenanthroline (99%) were purchased from Shanghai
8 Aladdin Biochemical Technology Co., Ltd. Cyanamide (CA) (99%) was produced from Shanghai
9 Macklin Biochemical Technology Co., Ltd. Pt/C catalyst (30 wt.%) was purchased from TANAKA.
10 Iridium black (99.8%, metals basis) was purchased from Alfa Aesar. Nafion® perfluorinated resin
11 solution (5 wt.%) in a mixture of lower aliphatic alcohols and 45% water was procured from Sigma-
12 Aldrich. Zn foil (0.2 mm thickness, 99.99%) and P3-type composite electrode substrate (0.3 mm
13 thickness) for zinc-air batteries were purchased from Changsha Spring New Energy Technology Co.,
14 Ltd. Ultrapure water ($18.2 \text{ M}\Omega \cdot \text{cm}$) was used throughout all the experiments.

15 Characterizations

16 Powder X-ray diffraction (PXRD) tests were carried out on a Bruker D8 diffractometer (Bruker
17 AXS, Karlsruhe, Germany) with $\text{Cu-K}\alpha$ radiation ($\lambda = 1.5418 \text{ \AA}$). The morphology of the catalysts
18 was measured by FEI Verios G4 UC Scanning Electron Microscope (SEM). High-resolution
19 transmission electron microscopy (HRTEM) images and energy dispersive X-ray analysis (EDX)
20 were performed on an FEI Talors F200i transmission electron microscope at an accelerating voltage
21 of 200 kV. The aberration-corrected high-angle annular dark-field scanning transmission electron
22 microscope (AC-HAADF-STEM) images were performed on JEM-ARM 200-F. Raman spectra
23 were performed on a confocal Raman microscope (WITec alpha 300R) in a range from 2000 to 800
24 cm^{-1} . N_2 adsorption-desorption isotherms were measured by using an adsorption instrument (ASAP
25 2460, Micromeritics Instrument Corp) at 77-K to evaluate the pore structures of catalysts. The
26 Brunauer-Emmett-Teller (BET) method was employed for the determination of the specific surface

1 area of the catalysts and the Barrett-Joyner-Halenda (BJH) model was employed to analyze the pore
2 size distribution and pore volume. X-ray photoelectron spectroscopy (XPS) measurements were
3 carried out on a Thermo Scientific ESCALAB 250 electron spectrometer to analyze surface
4 chemistry. All of the XPS results are calibrated by the peak position of C 1s spectra (284.8 eV).
5 Inductively coupled plasma optical emission spectroscopy (ICP-OES) was performed on an Agilent
6 7900 ICP-MS.

7 Electrochemical Measurements

8 Electrochemical measurements were carried out on a standard three-electrode system with a CHI
9 760E electrochemical workstation (CH Instruments, China). A graphite rod and a calibrated
10 saturated calomel electrode served as the counter electrode and the reference electrode, respectively.
11 The Hg/HgO reference electrode was calibrated concerning the reversible hydrogen electrode (RHE)
12 before use. The calibration was performed in a hydrogen-saturated KOH solution at 25 ± 1 °C with
13 Pt foil as the working electrode and counter electrode. The result in different pH solutions is shown
14 in Fig. S1, $E(\text{RHE}) = E(\text{Hg/HgO}) + 0.8905 \text{ V}$ (in 0.1 M KOH), respectively. A polished glassy
15 carbon rotating disk electrode (RDE, 5mm in diameter) or rotating ring disk electrode (RRDE, 5.6
16 mm in diameter) with catalyst inks coated on it was used as the working electrode. To prepare the
17 working electrode, 5 mg of the catalyst was dispersed into 950 μL isopropanol and 20 μL Nafion[®]
18 under ultrasonication for 30 minutes to form the uniform ink. After that, 15 μL of the prepared ink
19 was dropped on the working electrode and dried naturally. The corresponding loading mass was
20 calculated to be $0.38 \text{ mg}\cdot\text{cm}^{-2}$. For comparison, a commercial 30 wt.% Pt/C electrocatalyst (TKK)
21 was used with a loading of $0.076 \text{ mg}\cdot\text{cm}^{-2}$. The final working electrode was obtained after drying at
22 room temperature. Before the measurement, the electrolyte was O₂-saturated in 0.1 M KOH for
23 ORR. The working electrode was cycled at $100 \text{ mV}\cdot\text{s}^{-1}$ until the curves were stable and then the
24 measurement curves were recorded.

25 The electron transfer number (n) was calculated by Koutecky-Levich (K-L) Equations (1) and (2):

$$\frac{1}{j} = \frac{1}{j_k} + \frac{1}{j_d} = \frac{1}{j_k} + \frac{1}{BC_0\omega^{\frac{1}{2}}} \quad (1)$$

26

$$B = 0.2nC_0(D_0)^{\frac{2}{3}}v^{-\frac{1}{6}} \quad (2)$$

where J is the measured current density, J_K and J_L are the kinetic-limiting current densities and diffusion-limiting current densities, respectively, and ω is the angular velocity of the disk. B represents the inverse slope of K-L plots, F is the Faraday constant ($96485 \text{ C}\cdot\text{mol}^{-1}$), C_0 is the bulk concentration of O_2 ($1.21 \times 10^{-3} \text{ mol}\cdot\text{L}^{-1}$), D_0 is the diffusion coefficient of O_2 ($1.9 \times 10^{-5} \text{ cm}^2\cdot\text{s}^{-1}$), and v is the kinematic viscosity of the electrolyte ($0.01 \text{ cm}^2\cdot\text{s}^{-1}$).

The n and H_2O_2 yield were calculated by the following Equations (3) and (4):

$$n = 4 * \frac{I_d}{\left(\frac{I_r}{N}\right) + I_d} \quad (3)$$

$$\text{H}_2\text{O}_2(\%) = 200 * \frac{I_r}{\left(\frac{I_r}{N}\right) + I_d} \quad (4)$$

where I_d is the disk current, I_r is the ring current, and N is the current collection efficiency of the Pt ring, which equals 0.249.

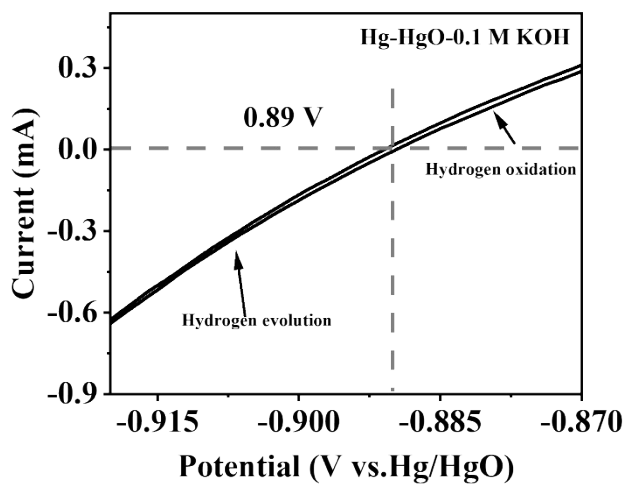
12 Fabrication and Measurements of Zn-air Battery

13 To fabricate the liquid Zn-air batteries (ZABs), the FeZn-NC-800 + Ir or commercial Pt/C + Ir
 14 coated on Nickel foam and carbon cloth composite substrates were used as the air cathodes, polished
 15 zinc foil as the anode, and aqueous solution containing 6 M KOH + 0.2 M $\text{Zn}(\text{CH}_3\text{COO})_2$ as the
 16 electrolyte. The mass loading of FeZn-NC-800 + Ir catalyst on the substrate was $2.5 \text{ mg}\cdot\text{cm}^{-2}$ (the
 17 same mass for both samples), the mass loading of Pt/C+ Ir was $2 \text{ mg}\cdot\text{cm}^{-2}$ (the same mass for both
 18 samples), and the effective geometrical area of the carbon cloth exposed to the electrolyte was 1.0
 19 cm^2 . The charge-discharge polarization curves were measured using CHI 760E electrochemical
 20 workstation. LANHE testing system was used to test the stability of the current charge and discharge
 21 cycle at a current density of $10 \text{ mA}\cdot\text{cm}^{-2}$ (discharge for 10 minutes and charge for 10 minutes as a
 22 charge-discharge cycle). LANHE testing system was also used to evaluate the performance of
 23 galvanostatic discharge at a current density of $10 \text{ mA}\cdot\text{cm}^{-2}$.

24

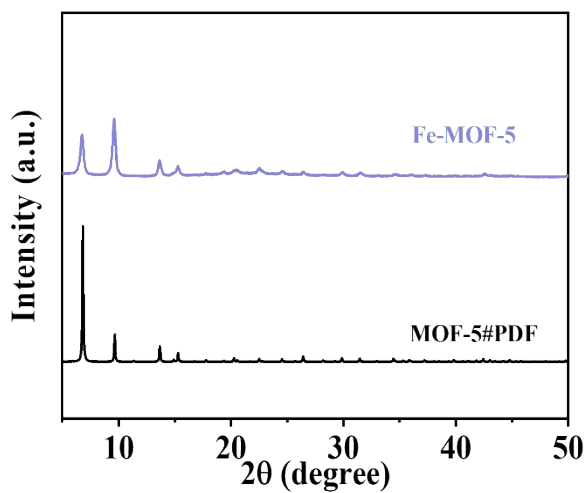
1 Supplementary Figures

2



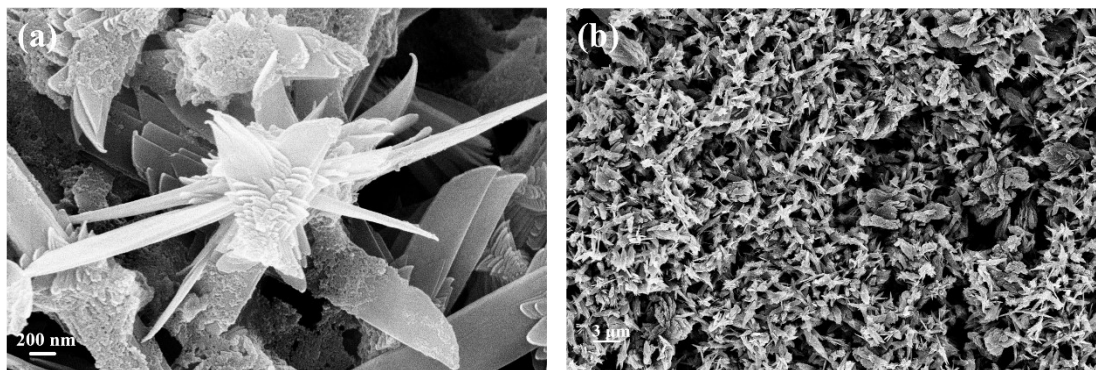
3

4 **Fig. S1.** Reversible hydrogen electrode (RHE) test in a hydrogen-saturated 0.1 M KOH solution at 25 ± 1
5 °C.



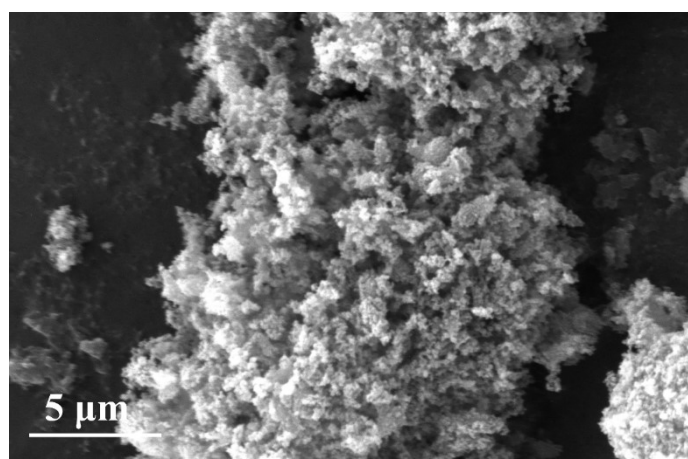
6

7 **Fig. S2.** XRD patterns of Fe-MOF-5 and MOF-5 standard cards.



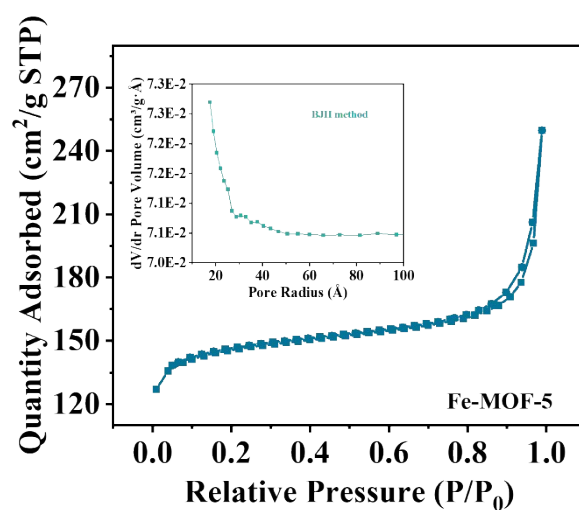
1

2 **Fig. S3.** (a-b) The SEM images of the Fe-MOF-5 at different magnifications.



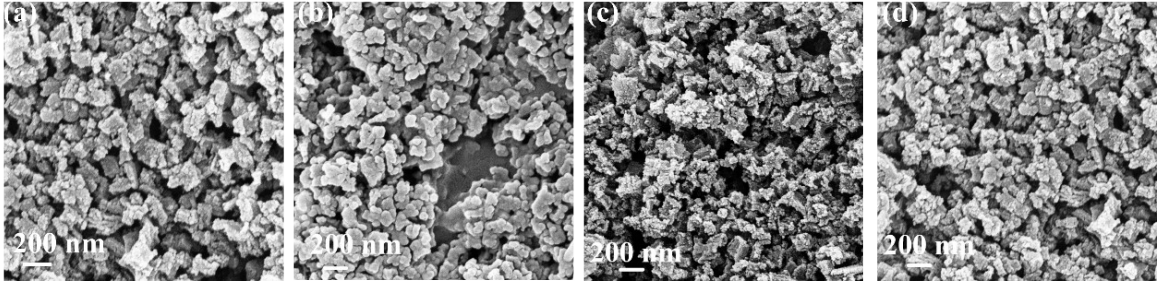
3

4 **Fig. S4.** SEM images of the Fe-MOF-5-precursor (without added PVP).



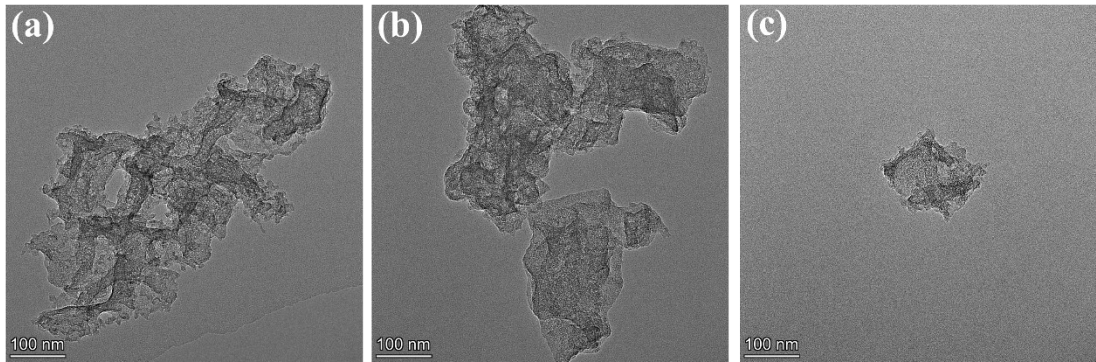
5

6 **Fig. S5.** The BET profile of the Fe-MOF-5 precursor, and the inset show the pore size distribution map of
7 the BJH method.



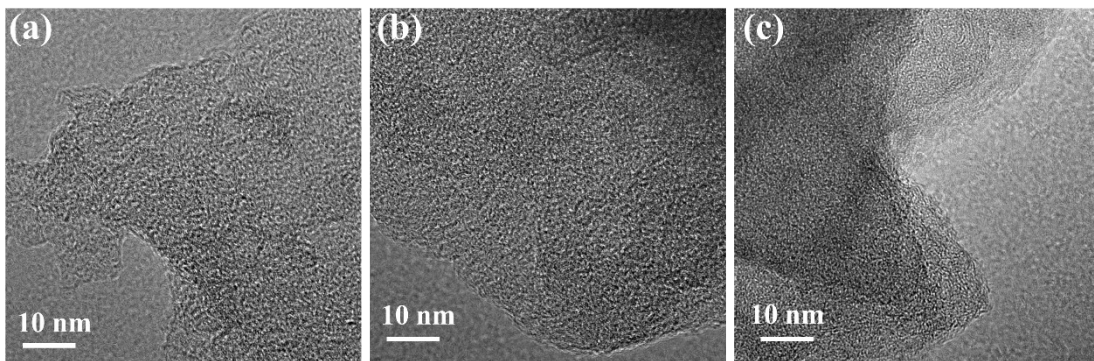
1

2 **Fig. S6.** SEM plots of (a) FeZn-NC-800, (b) FeZn-NC-800_{w/o-CA}, (c) FeZn-NC-700, and (d) FeZn-NC-900
3 at 200 nm.



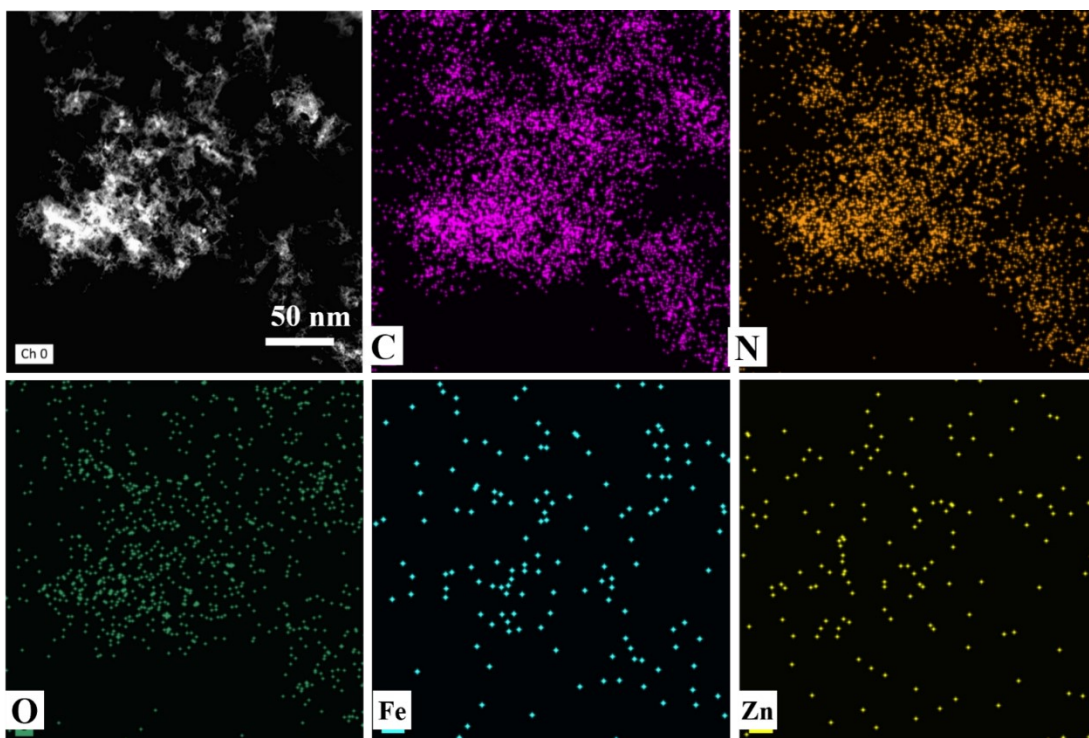
4

5 **Fig. S7.** TEM plots of (a) FeZn-NC-800_{w/o-CA}, (b) FeZn-NC-700, and (c) FeZn-NC-900 at 100 nm.



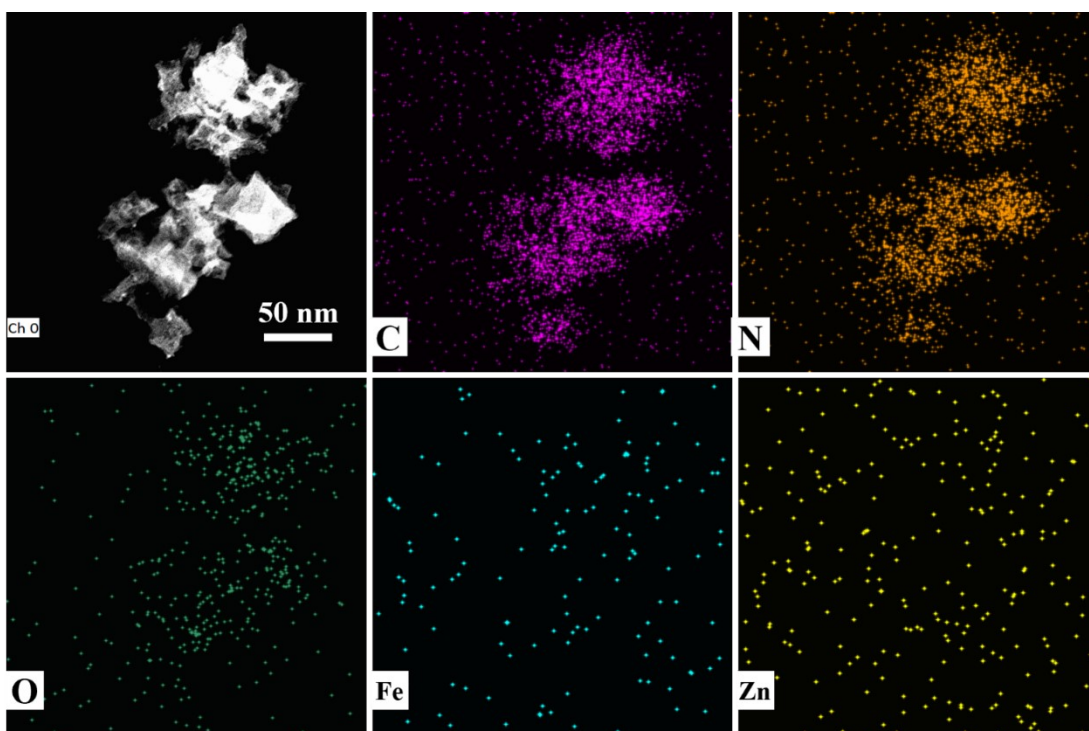
6

7 **Fig. S8.** TEM plots of (a) FeZn-NC-800_{w/o-CA}, (b) FeZn-NC-700, and (c) FeZn-NC-900 at 10 nm.



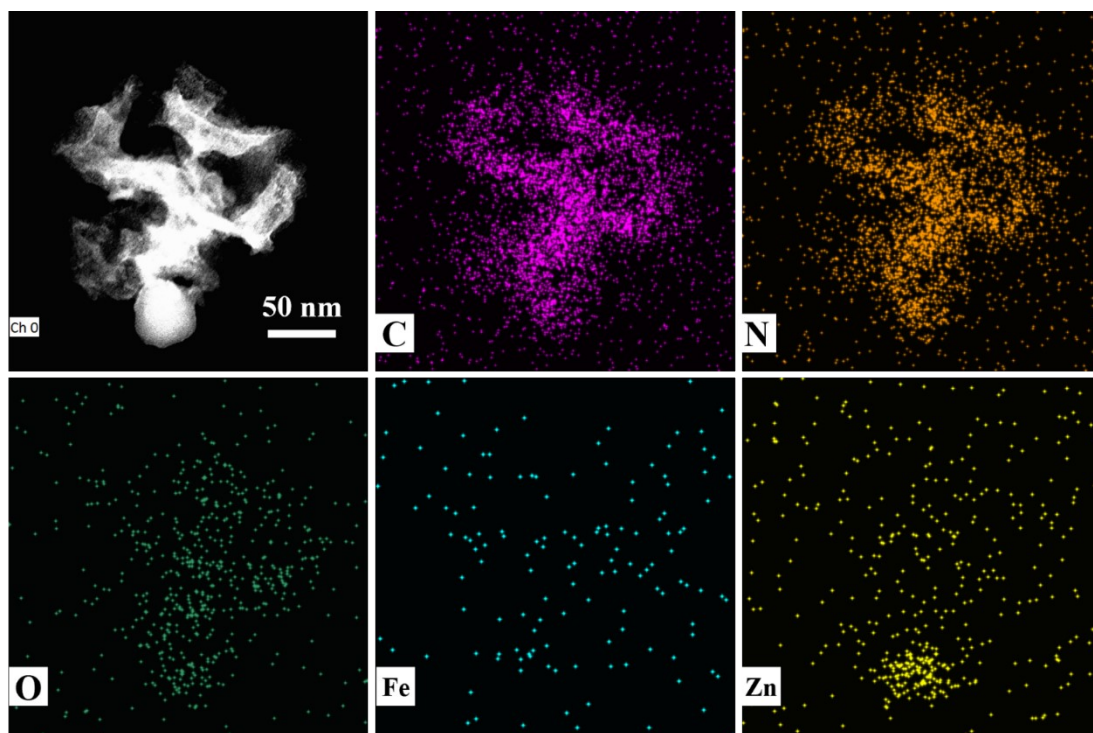
1

2 **Fig. S9.** HAADF-STEM and EDS elemental mapping images for C, N, O, Fe, and Zn of the FeZn-NC-
 3 800_{w/o-CA}. Scale bars in d: 50 nm.



4

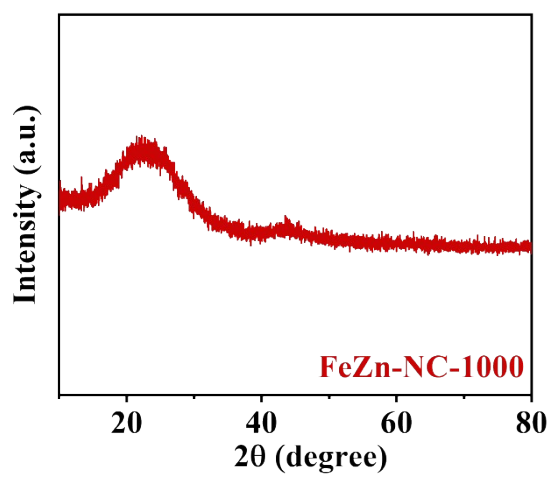
5 **Fig. S10.** HAADF-STEM and EDS elemental mapping images for C, N, O, Fe, and Zn of the FeZn-NC-700.
 6 Scale bars in d: 50 nm.



1

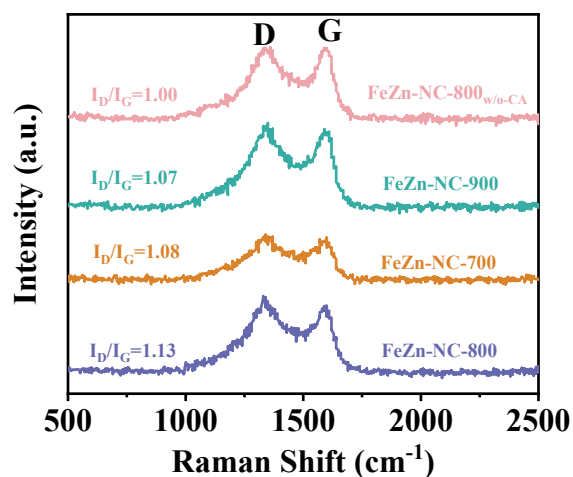
2 **Fig. S11.** HAADF-STEM and EDS elemental mapping images for C, N, O, Fe, and Zn of the FeZn-NC-900.

3 Scale bars in d: 50 nm.



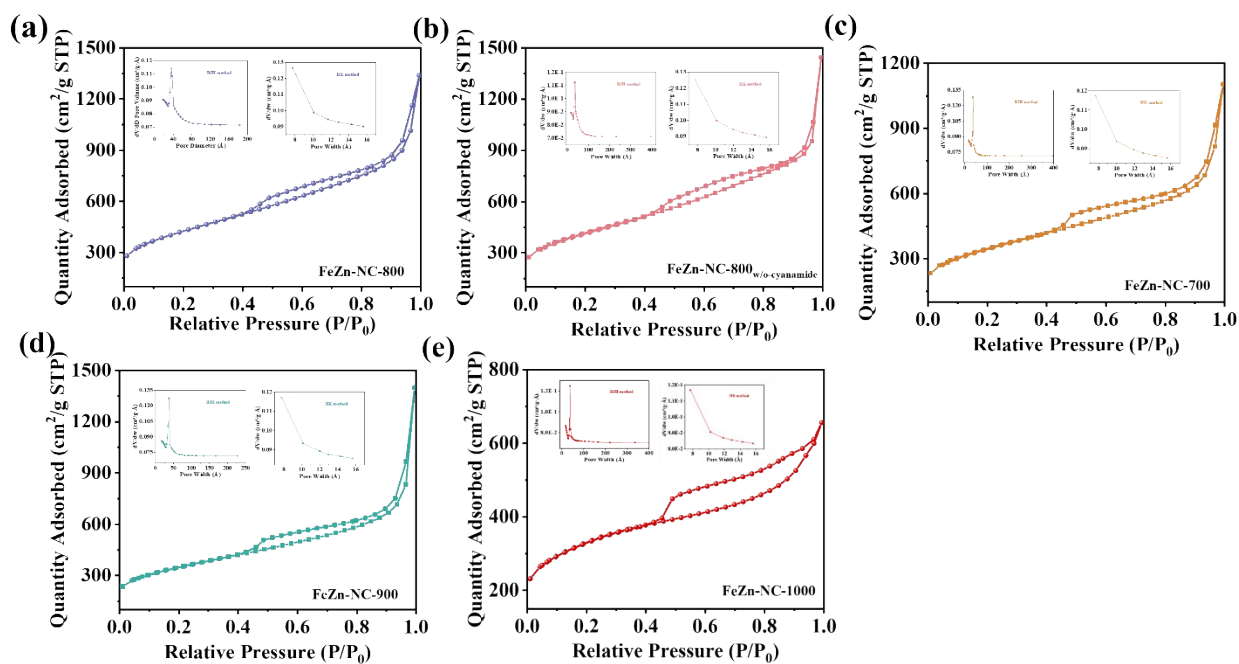
4

5 **Fig. S12.** XRD pattern of FeZn-NC-1000 catalyst.



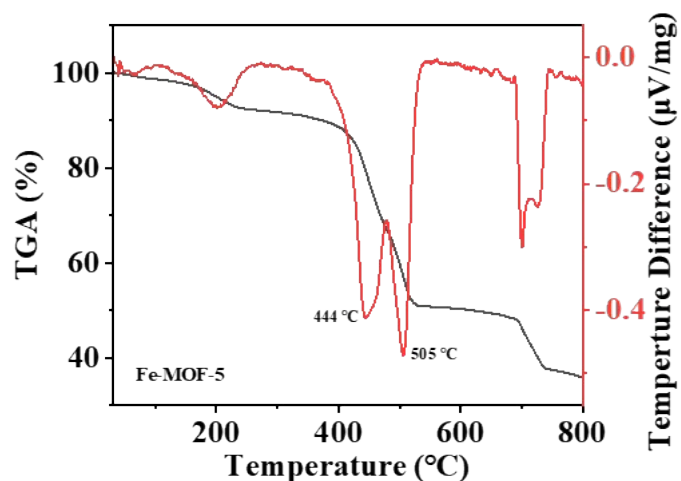
1

2 **Fig. S13.** Raman spectra of FeZn-NC-800, FeZn-NC-800_{w/o-CA}, FeZn-NC-700, and FeZn-NC-900 catalysts.



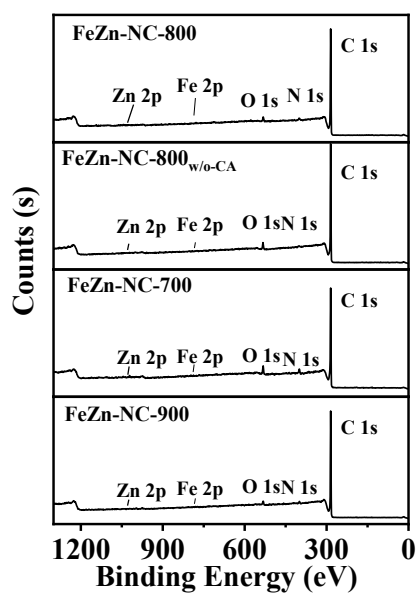
3

4 **Fig. S14.** N₂ adsorption/desorption isotherms at 77 K, and the related pore size distribution plots by BJH
 5 method and HK method analysis of (a) FeZn-NC-800, (b) FeZn-NC-800_{w/o-CA}, (c) FeZn-NC-700, (d) FeZn-
 6 NC-900 and (e) FeZn-NC-1000 catalysts.



1

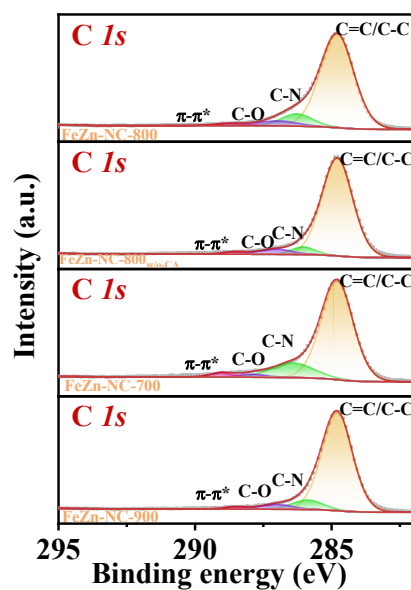
2 **Fig. S15.** TG-DSC curves of the Fe-MOF-5 precursor.



3

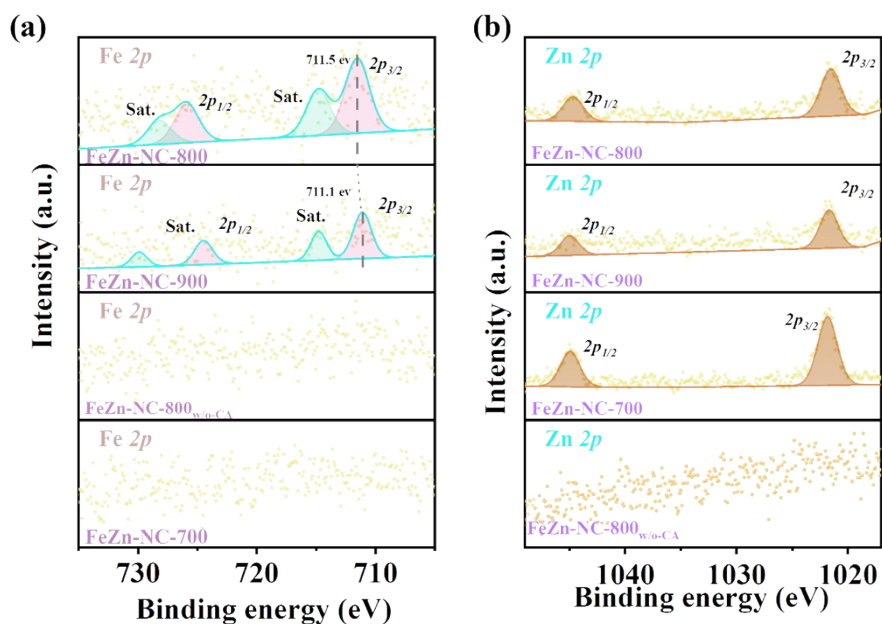
4 **Fig. S16.** XPS survey scan of FeZn-NC-800, FeZn-NC-800_{w/o-CA}, FeZn-NC-700, and FeZn-NC-900

5 catalysts.



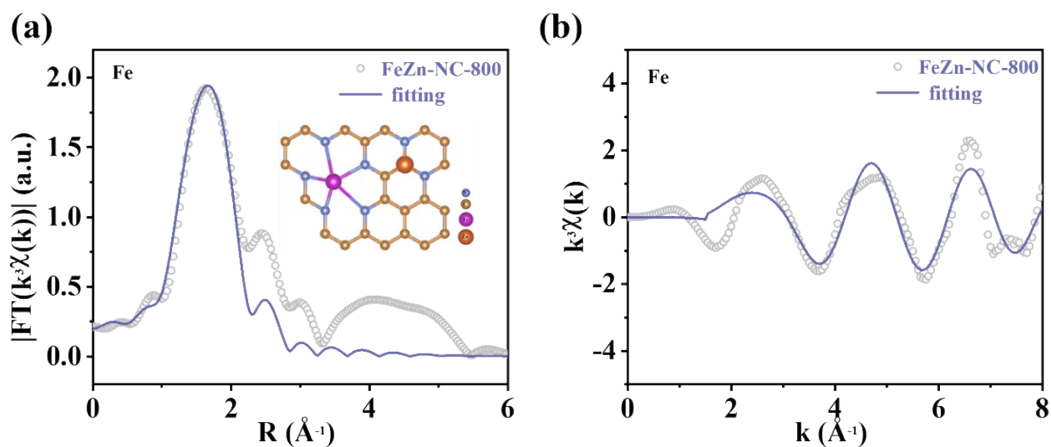
1

2 **Fig. S17.** High-resolution C 1s spectra of FeZn-NC-800, FeZn-NC-800_{w/o-CA}, FeZn-NC-700, and FeZn-NC-
3 900 catalysts.



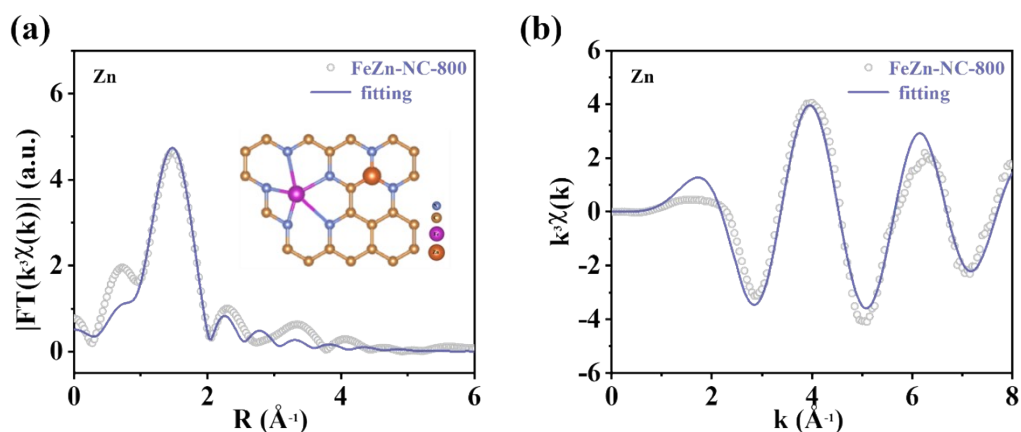
4

5 **Fig. S18.** High-resolution (a) Fe 2p and (b) Zn 2p spectra of FeZn-NC-800, FeZn-NC-800_{w/o-CA}, FeZn-NC-
6 700, and FeZn-NC-900 catalysts.



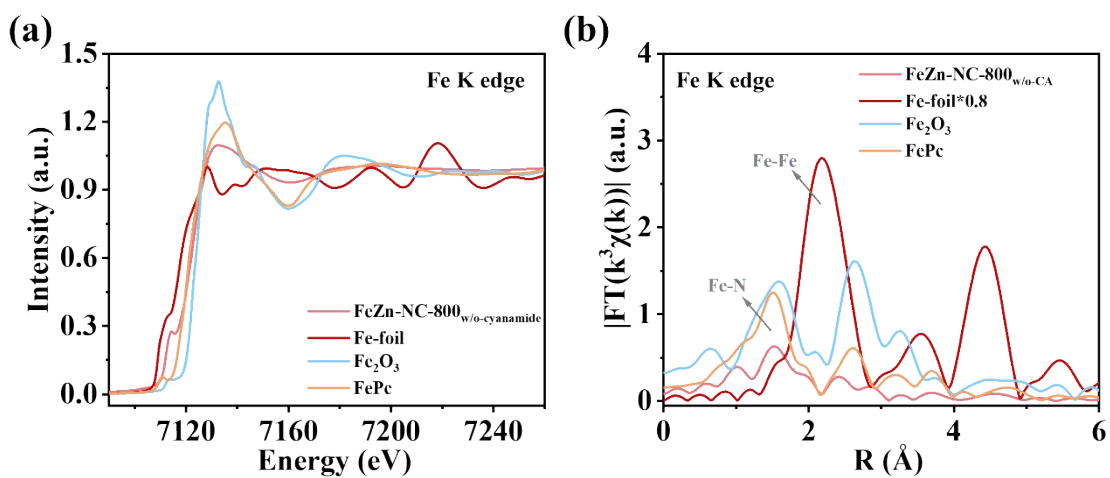
1

2 **Fig. S19.** (a) Corresponding EXAFS fitting curves at the Fe K-edge of FeZn-NC-800. (b) K-space
3 oscillations of different coordinated atoms.



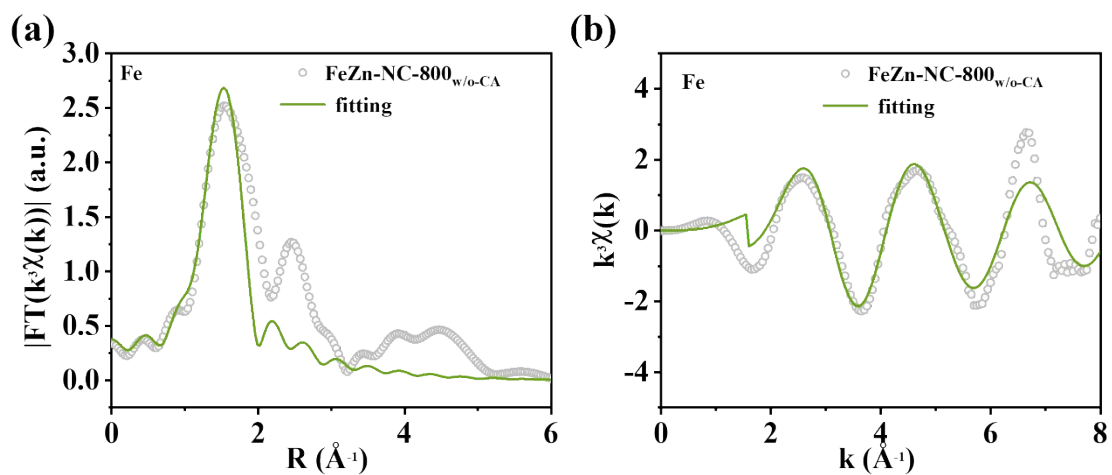
4

5 **Fig. S20.** (a) Corresponding EXAFS fitting curves at the Zn K-edge of FeZn-NC-800. (b) K-space
6 oscillations of different coordinated atoms.



7

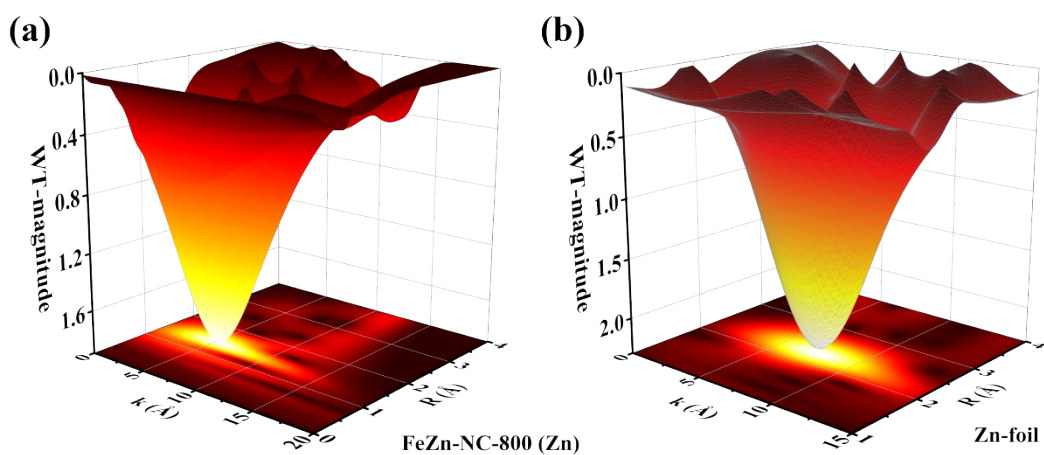
8 **Fig. S21.** (a) Fe K-edge XANES spectra and (b) FT-EXAFS spectra in FeZn-NC-800_{w/o-CA}.



1

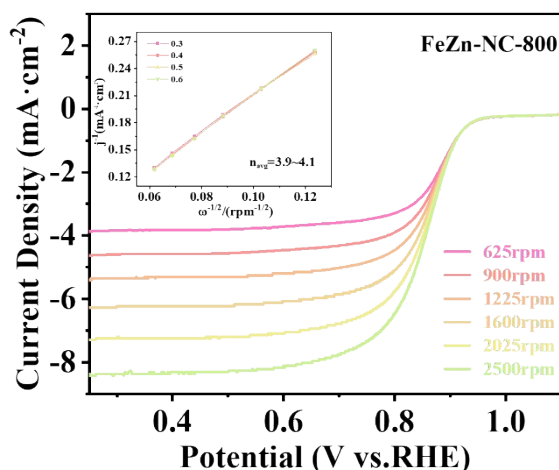
2 **Fig. S22.** (a) Corresponding EXAFS fitting curves at the Fe K-edge of FeZn-NC-800_{w/o-CA}. (b) K-space
 3 oscillations of different coordinated atoms.

4



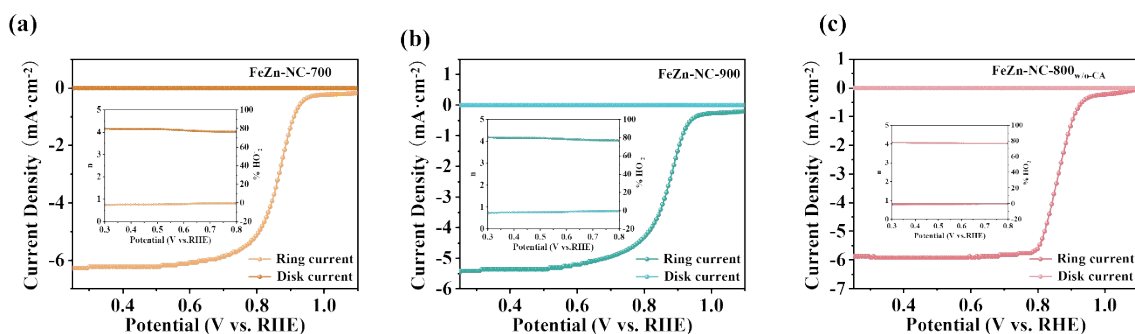
5

6 **Fig. S23.** Wavelet transform of k^3 -weighted EXAFS data of Zn K-edge in (a) FeZn-NC-800 and (b) Zn-foil.



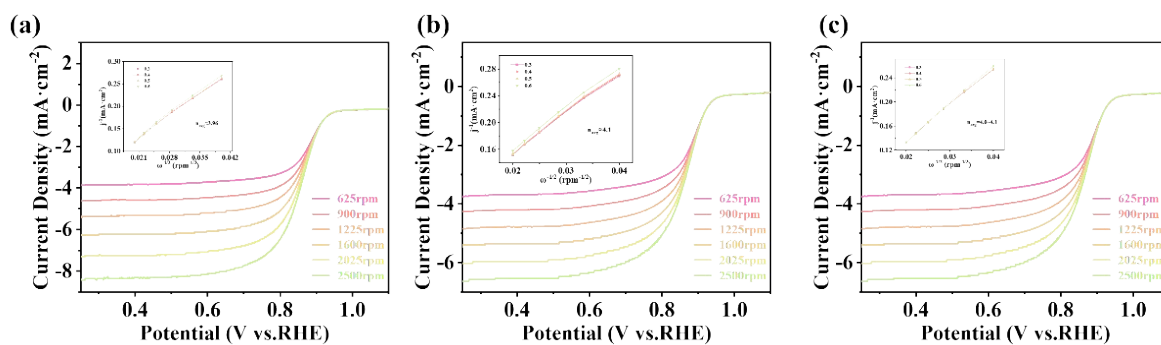
1

2 **Fig. S24.** LSV of FeZn-NC-800 at different rotation speeds, with an inset showing the number of transferred
 3 electrons.



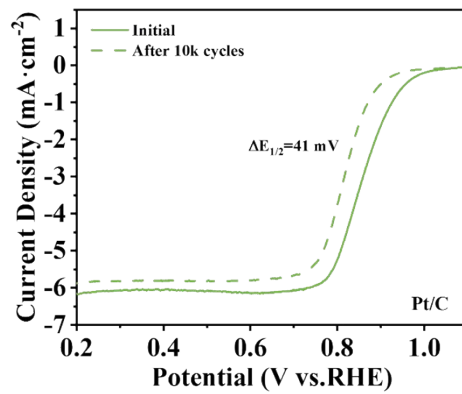
4

5 **Fig. S25.** H₂O₂ yield and electron transfer number of FeZn-NC-700、FeZn-NC-900 and FeZn-NC-800_{w/o-}
 6 CA.



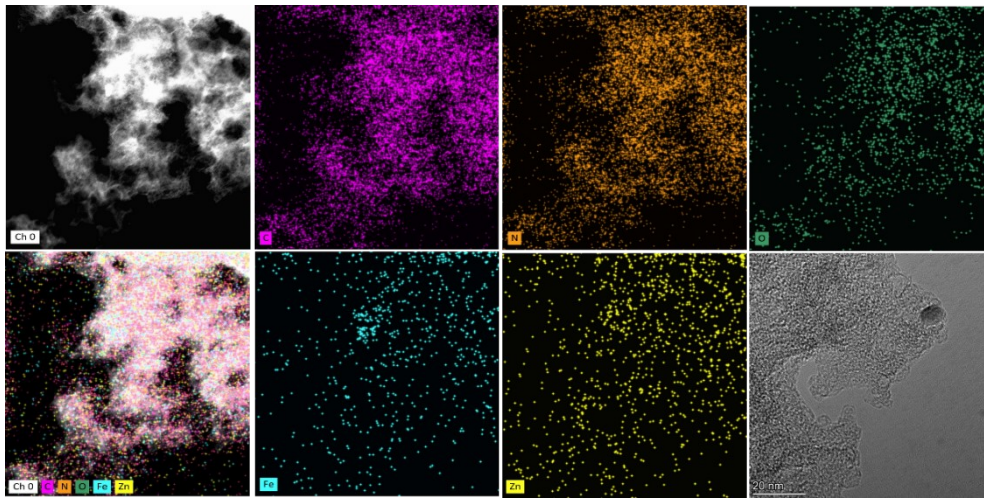
7

8 **Fig. S26.** LSV of FeZn-NC-700、FeZn-NC-900 and FeZn-NC-800_{w/o-CA} at different rotation speeds, with
 9 an inset showing the number of transferred electrons.



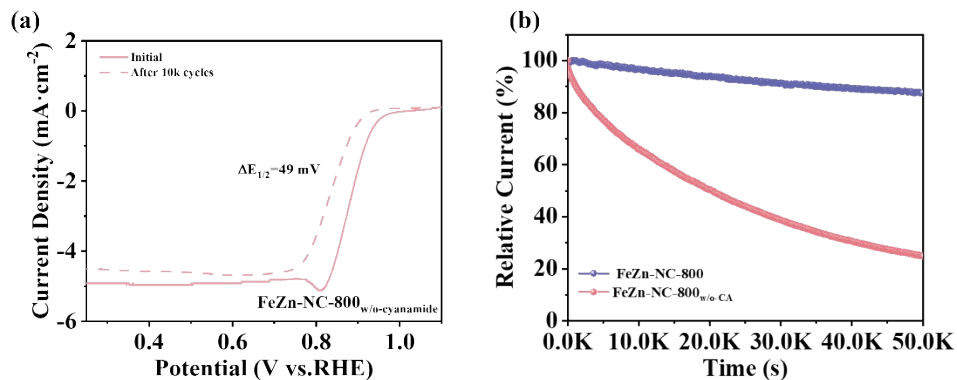
1

2 **Fig. S27.** Repeat testing of the LSV curve before and after 10000 cycles CV for Pt/C.



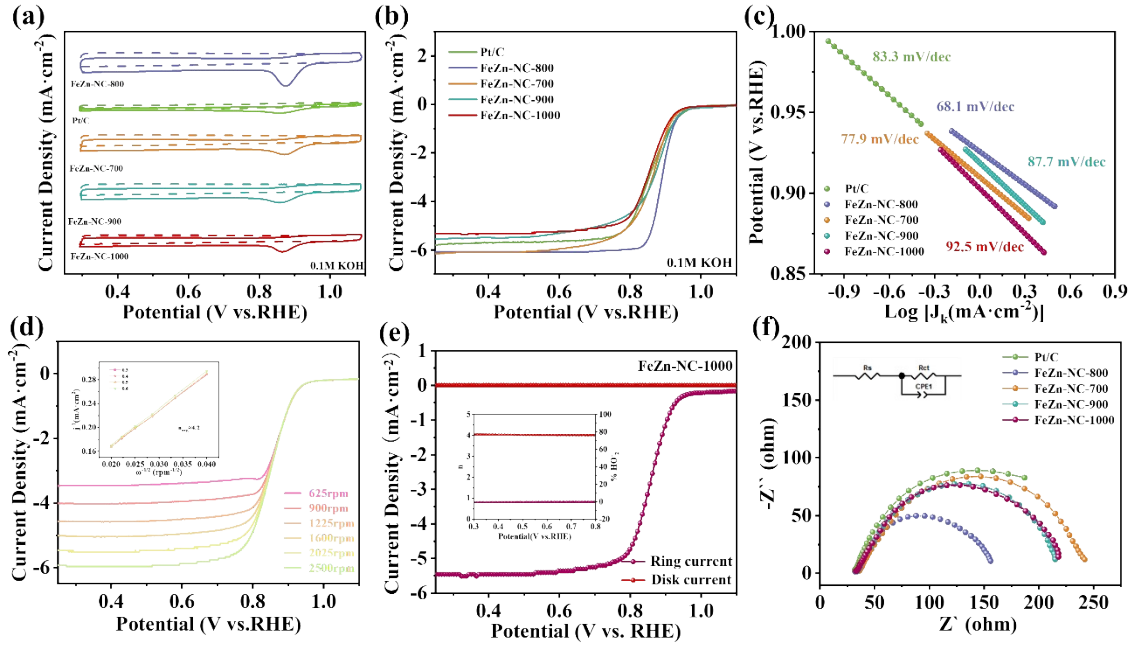
3

4 **Fig. S28.** HAADF-STEM and EDS elemental mapping images of C, N, O, Fe, and Ni in FeZn-NC-800 after
 5 stability testing. The scale bar is d: 50 nm.



6

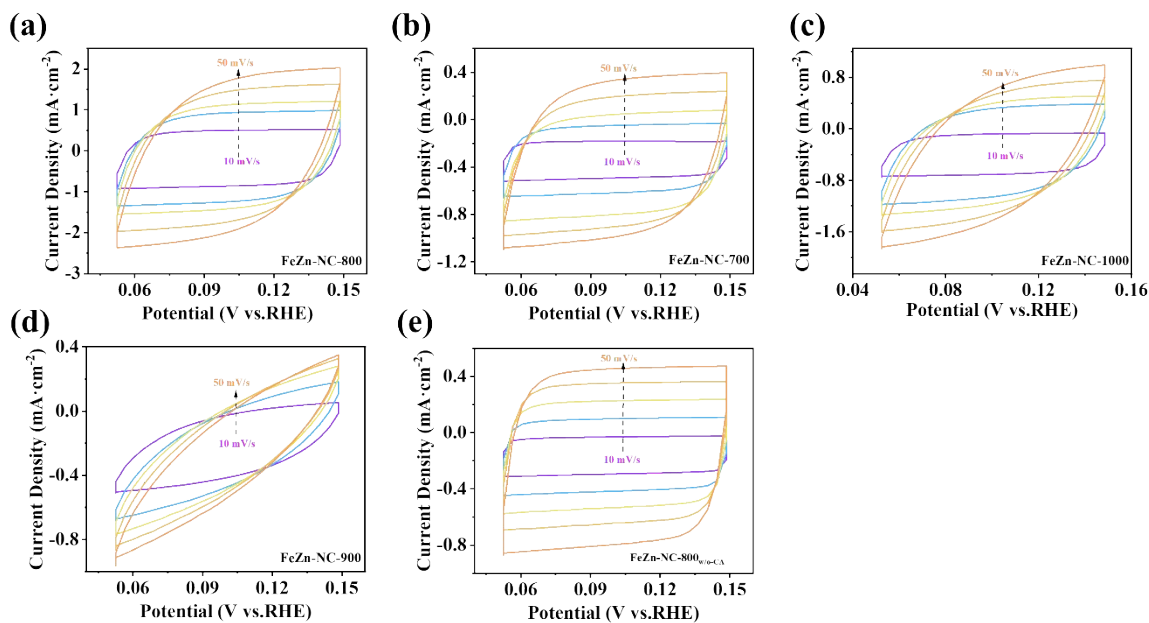
7 **Fig. S29.** (a) repeat testing of the LSV curve before and after 10000 CV for FeZn-NC-800_{w/o-CA}. (b)
 8 Normalized chronoamperometry curves at constant potentials of $E_{1/2}$ for catalysts (FeZn-NC-800_{w/o-CA} and
 9 FeZn-NC-800).



1

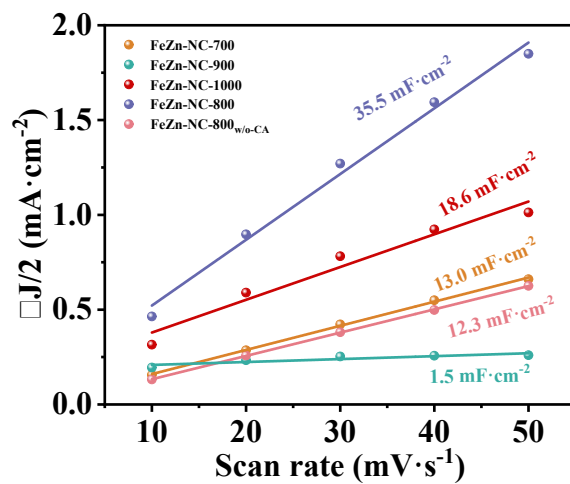
2 **Fig. S30.** The ORR electrochemical properties. (a) CV curves were measured in N_2 -saturated and O_2 -
 3 saturated atmospheres of FeZn-NC-800、FeZn-NC-700、FeZn-NC-900、FeZn-NC-1000 and Pt/C.
 4 (b) LSV curves in O_2 -saturated 0.1 M KOH solution at 1600 rpm of FeZn-NC-800、FeZn-NC-700、FeZn-
 5 NC-900、FeZn-NC-1000 and Pt/C. (c) Tafel slope of FeZn-NC-800、FeZn-NC-700、FeZn-NC-900、
 6 FeZn-NC-1000 and Pt/C. (d) LSV of FeZn-NC-1000 at different rotation speeds, with an inset showing the
 7 number of transferred electrons. (e) H_2O_2 yield and electron transfer number of FeZn-NC-1000. (f) Nyquist
 8 plots of various catalysts with frequency from 0.01 to 10^5 of FeZn-NC-800, FeZn-NC-700, FeZn-NC-900,
 9 FeZn-NC-1000 and Pt/C.

10



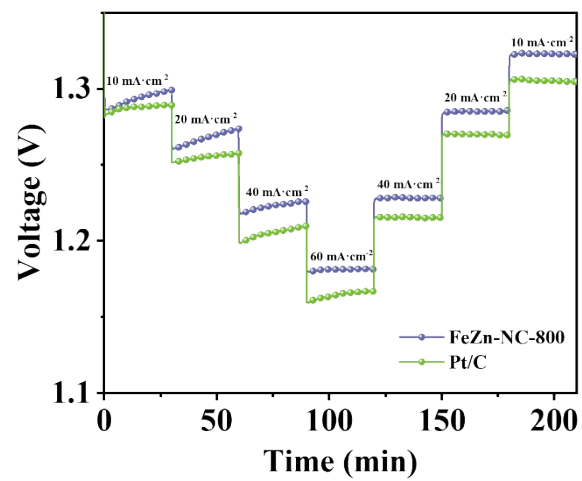
1

2 **Fig. S31.** CV curves from 0.05 to 0.15 V vs. RHE in 0.1 M KOH solution at scan rates of 10, 20, 30, 40 and
 3 50 $\text{mV}\cdot\text{s}^{-1}$, respectively. (a) FeZn-NC-800, (b) FeZn-NC-700, (c) FeZn-NC-1000 (d) FeZn-NC-900 and (e)
 4 FeZn-NC-800_{w/o-CA}.



5

6 **Fig. S32.** Dependence of current densities as a function of scan rates at 0.25 V vs. RHE.



1

2 **Fig. S33.** Galvanostatic discharge plots at various current densities for the ZABs assembled with FeZn-NC-

3 800 and Pt/C catalysts.

1 Supplementary Tables

2 **Table S1.** The Fe and Zn contents were determined by ICP-MS analysis.

Catalysts	Fe (wt.%)	Zn (wt.%)
FeZn-NC-800	0.414	0.871
FeZn-NC-800 _{w/o-CA}	0.414	0.097
FeZn-NC-700	0.543	0.418
FeZn-NC-900	0.401	0.611

3

4 **Table S2.** Summary of BET surface area and average pore diameter analysis of as-synthesized electrocatalysts.

Catalysts	BET Surface Area (m ² /g)	Average pore diameter (4V/A by BET) (nm)	HK method median pore width (nm)
FeZn-NC-800	1481.51	3.85	0.775
FeZn-NC-800 _{w/o-CA}	1448.07	3.76	0.775
FeZn-NC-700	1190.56	3.69	0.766
FeZn-NC-900	1196.06	3.70	0.776
FeZn-NC-1000	1109.76	3.22	0.771

5

6 **Table S3.** Elemental contents of C, N, O, Fe, and Zn based on XPS analysis for different samples.

Catalysts	C (at. %)	O (at. %)	N (at. %)	Fe (at. %)	Zn (at. %)
FeZn-NC-800	94.68	2.39	2.50	0.25	0.19
FeZn-NC-800 _{w/o-CA}	94.77	3.26	1.74	0.18	0.05
FeZn-NC-700	90.97	4.22	4.38	0.08	0.35
FeZn-NC-900	95.32	2.28	2.08	0.16	0.15

7

1 **Table S4.** Summary of the nitrogen species and their content of various synthetic electrocatalysts.

Catalysts	Pyrrolic-N (at. %)	Pyridinic-N (at. %)	Graphitic-N (at. %)	M-N _x (at. %)
FeZn-NC-800	28.81	47.98	7.65	15.56
FeZn-NC-800 _{w/o-CA}	33.52	21.59	19.72	25.17
FeZn-NC-700	19.38	43.92	20.65	16.05
FeZn-NC-900	20.97	46.45	18.13	14.15

2

3 **Table S5.** EXAFS fitting structure parameters of FeZn-NC-800.

Bond	CN	R/Å	$\sigma^2/\text{Å}^2$	R-factor	$\Delta E_0/\text{eV}$
Fe-N	2.1	1.975	0.012	0.011	8.0
Fe-C	1.2	2.486	0.002		
Zn-N	4.9	1.989	0.01	0.002	-2.12

4

5 **Table S6.** EXAFS fitting structure parameters of FeZn-NC-800_{w/o-CA}.

Bond	CN	R/Å	$\sigma^2/\text{Å}^2$	R-factor	$\Delta E_0/\text{eV}$
Fe-N	1.9	1.974	0.009	0.019	9.5

6

1 **Table S7.** Summary of the ORR activities of reported ORR catalysts in 0.1 M KOH.

Catalysts	$E_{1/2}$ (V vs. RHE)	E_{onset} (V vs. RHE)	Ref.
FeZn-NC-800	0.891	0.94	This work
Zn/Fe-NC	0.875	0.994	Appl. Catal. B 2023, 335 , 122875.
FeZn/N/C/MWCNT-800	0.858	0.966	J. Mater. Chem. A 2022, 10 , 3169-3177.
FeN ₅	0.854	0.971	Small 2023, 19 , e2300373.
SA-Fe/NG	0.88	0.9	PANS 2018, 115 , 6626-6631.
Fe-N/P-C-700	0.867	0.941	J. Am. Chem. Soc. 2020, 142 , 2404-2412.
FeCo-DACs/NC	0.877	0.984	Adv. Mater. 2022, 34 , 2107421.
FeNi SAs/NC	0.84	0.98	Adv. Energy Mater.2021, 11 , 2101242.
Fe-N-C HNSs	0.87	1.046	Adv. Mater. 2019, 31 , 180631.
Cu/Zn-NC	0.83	0.98	Angew. Chem. Int. Ed. 2021, 60 ,14005–14012.
Fe/OES	0.85	1.00	Angew. Chem. Int. Ed. 2020, 132 : 7454-7459.
SA&NP-FeCo-NTS	0.87	0.98	Adv. Funct. Mater. 2022, 32 , 2112805
CoNC-SAC	0.86	0.93	Sci. Adv. 2022, 8 , eabn5091.
Fe-Zn@SNC	0.87	-	Angew. Chem. Int. Ed. 2023, 62 : e202301833.
Fe/Zn-N-C	0.906	-	Energy Environ. Sci., 2022, 15 , 1601–1610
Fe-OAC	0.854	0.98	Appl. Catal. B: Environ., 2022, 305 , 121058.
Fe@NC(10+900)	0.82	0.94	Inorg. Chem. Front. 2022, 9 , 2557-2567.
Fe/Fe-N-C-3	0.87	0.97	J. Mater. Chem. A 2022, 10 , 20993-21003.
FeSA/N-PSCS	0.87	0.976	Energy Storage Mater. 2023, 59 , 102790.
Fe,N,P-CNSs/Fe ₂ P	0.854	0.955	Nano Energy 2023, 108 , 108179.
SA&NP-FeCo-NTS	0.87	0.98	Adv. Funct. Mater. 2022, 32 , 2112805
(Fe,Co)Se ₂ @Fe1/NC	0.88	-	Adv. Funct. Mater. 2023, 33 , 2300815.
Ni-N ₄ /GHSs/Fe-N ₄	0.83	-	Adv. Mater. 2022, 32 , 2003134.
A-SAC(Fe,Ni,Zn)/NC	0.88	0.92	Chem. Eng. J. 2023, 460 , 141868.
Fe ₂ Co/DSA-NSC	0.879	-	ACS Catal, 2023, 13 , 2313-2325.

2

1 **Table S8.** Comparison of the performance of rechargeable Zn-air batteries reported in recent literatures.

Catalysts	Peak power density (mW·cm ⁻²)	Specific capacity (mAh·g ⁻¹)	Stability	Ref.
FeZn-NC-800	218.1	751.55 @10 mA·cm ⁻²	10 mA cm ⁻² for 200 h	This work
Zn/Fe-NC	186.8	807.5 @5 mA·cm ⁻²	-	Angew. Chem., Int. Ed. 2020, 132 , 7454–7459.
S-Cu-ISA/SNC	225	735 @ 10 mA·cm ⁻²	10 mA cm ⁻² for 45 h	Nat. Comm. 2020, 11 , 3049.
Fe-SAs/NPS-HC	195	-	5 mA cm ⁻² for 55.5 h	Nat. Comm. 2018, 9 , 5422.
Zn/Fe-NC	186.2	814.6 @ 10 mA·cm ⁻²	10 mA cm ⁻² for 50 h	Appl. Catal. B 2023, 335 , 122875.
A-FeCo@NCNs	132	736.2 @ 10 mA·cm ⁻²	2 mA cm ⁻² for 167 h	J. Catal. 2021, 397 , 223–232
FeNiCo@NC-P	112	-	10 mA cm ⁻² for 45 h	Adv. Funct. Mater. 2019, 30 , 1908167.
H ₂ PO ₂ /FeNi-LDH-V ₂ C	137	-	5 mA cm ⁻² for 100 h	Appl. Catal. B: Environ. 2021, 297 , 120474.
Fe-NiNC-50	200	932.66 @ 10mA·cm ⁻²	2 mA cm ⁻² for 100 h	Nano Energy 2020, 71 , 104597
Fe-NHC	157	755.8 @ 20 mA·cm ⁻²	10 mA cm ⁻² for 64 h	Appl. Catal. B: Environ., 2021, 285 , 119780.
Fe/FexC@Fe-N-C900	150	-	10 mA cm ⁻² for 65 h	Chem. Eng. J., 2023, 453 , 139820.
Fe/N-CNRs	181.5	771.8 @ 10 mA·cm ⁻²	10 mA cm ⁻² for 100 h	Adv. Funct. Mater., 2021, 31 , 2008085.
P-doped Fe-N-C	201	-	1 mA cm ⁻² for 600 h	ACS Nano, 2022, 16 , 15994–16002.
FeN ₃ @NMCNFs	158	790.2@ 10 mA·cm ⁻²	5 mA cm ⁻² for 150 h	Appl. Catal. B: Environ., 2025, 366 , 125007
B-FeNi-N/C-1000	102	-	10 mA cm ⁻² for 95 h	Chem. Eng. Sci., 2022 247 117038
FeNi-NCS-2	109.8	639.71@20 mA·cm ⁻²	10 mA cm ⁻² for 13 h	Int. J. Hydrogen Energy 2022 47 984-992.
Co _{SA-AC} @SNC	174.1	760.6@ 15 mA·cm ⁻²	15 mA cm ⁻² for 138 h	<i>Small</i> , 2024, 20 , 2402323.
Co@FeSAC-N ₂ P/C	179	-	5 mA cm ⁻² for 165 h	<i>Appl. Catal., B</i> , 2022, 313 , 121429
FePc-CoNC-CMS	147.6	631.1 @10 mA·cm ⁻²	10 mA cm ⁻² for 70 h	Adv. Funct. Mater., 2022, 32 , 2112805.
FePc@CNF	139.3	651.53@10 mA·cm ⁻²	-	Chem. Eng. Sci.,2024, 483 , 149243.

2